Supplemental Material can be found at:
http://www.jbc.org/content/suppl/2006/04/12/M601876200.DC1.html

THE JOURNAL OF BIOLOGICAL CHEMISTRY VOL. 281, NO. 24, pp. 16768–16776, June 16, 2006
© 2006 by The American Society for Biochemistry and Molecular Biology, Inc. Printed in the U.S.A.

Differential Metabolomics Reveals Ophthalmic Acid as an Oxidative Stress Biomarker Indicating Hepatic Glutathione Consumption*[S]

Received for publication, February 27, 2006, and in revised form, March 29, 2006 Published, JBC Papers in Press, April 11, 2006, DOI 10.1074/jbc.M601876200

Tomoyoshi Soga[‡§1,2], **Richard Baran**[‡1], **Makoto Suematsu**[¶1,3], **Yuki Ueno**[‡§], **Satsuki Ikeda**[‡], **Tadayuki Sakurakawa**[¶], **Yuji Kakazu**[‡], **Takamasa Ishikawa**[§], **Martin Robert**[‡], **Takaaki Nishioka**[‡], **and Masaru Tomita**[‡§]

From the [‡]*Institute for Advanced Biosciences, Keio University, Tsuruoka, Yamagata 997-0017, Japan,* [§]*Human Metabolome Technologies Inc., Tsuruoka, Yamagata 997-0017, Japan, and the* [¶]*Department of Biochemistry and Integrative Medical Biology, School of Medicine, Keio University, Shinanomachi, Shinjuku-ku, Tokyo 160-8582, Japan*

Metabolomics is an emerging tool that can be used to gain insights into cellular and physiological responses. Here we present a metabolome differential display method based on capillary electrophoresis time-of-flight mass spectrometry to profile liver metabolites following acetaminophen-induced hepatotoxicity. We globally detected 1,859 peaks in mouse liver extracts and highlighted multiple changes in metabolite levels, including an activation of the ophthalmate biosynthesis pathway. We confirmed that ophthalmate was synthesized from 2-aminobutyrate through consecutive reactions with γ-glutamylcysteine and glutathione synthetase. Changes in ophthalmate level in mouse serum and liver extracts were closely correlated and ophthalmate levels increased significantly in conjunction with glutathione consumption. Overall, our results provide a broad picture of hepatic metabolite changes following acetaminophen treatment. In addition, we specifically found that serum ophthalmate is a sensitive indicator of hepatic GSH depletion, and may be a new biomarker for oxidative stress. Our method can thus pinpoint specific metabolite changes and provide insights into the perturbation of metabolic pathways on a large scale and serve as a powerful new tool for discovering low molecular weight biomarkers.

An excess dose of acetaminophen (AAP),[4] the most commonly used analgesic, can lead to possibly fatal hepatitis and more than 100 such deaths occur in the United States annually. AAP is normally detoxified by sulfation or glucoronidation followed by elimination (1). In high doses, it is metabolized by P450 cytochromes to generate the reactive intermediate *N*-acetyl-*p*-benzoquinone imine (NAPQI) (2), which is further inactivated by conjugation with glutathione (GSH) before excretion. This results in a sudden drop in GSH levels (3). In absence of sufficient GSH, the reactive NAPQI can cause toxic and covalent protein modifications that lead to cell death and tissue injury (4–7).

Recent transcriptomic and proteomic studies showed that AAP can cause numerous changes in gene and protein expression levels in pathways related to cellular stress response, mitochondrial function, and metabolism, as well as in cell cycle, structural, signaling, and apoptotic proteins (8, 9). However, little is known about global changes in metabolites. Global information about when and where metabolite levels increase or decrease can reveal connections in biological networks and provide a system level understanding of the cell (10–14). However, unlike other functional genomic approaches, metabolome analysis methods are still under development. Current large scale metabolite analysis methods are based on gas chromatography mass spectrometry (15), liquid chromatography mass spectrometry (LC-MS) (16), NMR (17), Fourier transform ion cyclotron resonance mass spectrometry) (18), and capillary electrophoresis mass spectrometry (CE-MS) (19). Whereas these analytical tools allow global metabolite profiling, the exploration and identification of changes in compounds among the enormous amount of data generated are laborious.

Here, we propose a novel strategy to analyze and differentially display metabolic profiles by coupling capillary electrophoresis with electrospray ionization time-of-flight mass spectrometry (CE-TOFMS). Using this profiling system, we determined global changes in metabolite levels in the liver and serum of AAP-treated mice, obtained insights into the perturbation of metabolic pathways related to hepatotoxicity, and identified biomarkers that can reveal acute liver injury.

MATERIALS AND METHODS

Animals and Drug Administration—Male C57BL6 mice, fasted overnight with free access to water, were anesthetized with an intraperitoneal (ip) injection of pentobarbital sodium (60 mg/kg). AAP or physiological saline as a vehicle was administered at 150 mg/kg. AAP was solubilized in saline prior to injection, to avoid the use of ethanol that could affect liver function. To achieve solubilization, AAP was added to warm saline kept at 42 °C followed by vortexing for 1 h. After the AAP injection, mice were allowed free access to chow diet and water. At the indicated times after AAP administration (1, 2, 4, 6, 12, and 24 h) the mice were anesthetized by urethane and were sacrificed to collect liver tissues and serum samples. The liver tissues were immediately snap-frozen in liquid nitrogen (20). In another set of experiments, diethylmaleate (DEM) or buthionine sulfoximine (BSO) (4 mmol/kg) was administered ip while the control mice were injected with physiological saline.

* This work was supported in part by a grant from the Ministry of Education, Culture, Sports, Science, and Technology (MEXT) (the 21st Century COE Program entitled "Understanding and Control of Life's Function via Systems Biology," and a grant from Grant-in-aid of Creative Researches and Leading Project for Biosimulation from MEXT in Japan as well as research funds from Yamagata prefectural government and Tsuruoka city. The costs of publication of this article were defrayed in part by the payment of page charges. This article must therefore be hereby marked "*advertisement*" in accordance with 18 U.S.C. Section 1734 solely to indicate this fact.

[S] The on-line version of this article (available at http://www.jbc.org) contains supplemental data.

[1] These authors contributed equally to this work.

[2] To whom correspondence may be addressed: Institute for Advanced Biosciences, Keio University, Tsuruoka, Yamagata 997-0017, Japan. Tel.: 81-235-29-0528; Fax: 81-0235-29-0530; E-mail: soga@sfc.keio.ac.jp.

[3] To whom correspondence may be addressed: Dept. of Biochemistry and Integrative Medical Biology, School of Medicine, Keio University, Shinanomachi, Shinjuku-ku, Tokyo 160-8582, Japan. E-mail: msuem@sc.itc.keio.ac.jp.

[4] The abbreviations used are: AAP, acetaminophen; CE-TOFMS, capillary electrophoresis time-of-flight mass spectrometry; 2AB, 2-aminobutyrate; GCS, γ-glutamylcysteine synthetase; GS, glutathione synthetase; ip, intraperitoneal; DEM, diethylmaleate; BSO, buthionine sulfoximine; MES, 2-morpholinoethanesulfonate; Oct RFV, octapole radio frequency voltage; ESI-Q-TOFMS, electrospray ionization quadrupole time-of-flight mass spectrometry; PIPES, piperazine-1,4-bis(2-ethansulfonate).

Downloaded from www.jbc.org at Biomedical Library, UCSD, on February 25, 2011

At the above time points post-administration, livers and serum samples were collected for metabolome analysis.

Metabolite Extraction—Frozen liver tissue (~300 mg) was immediately plunged into methanol (1 ml) containing internal standards (300 μM each of methionine sulfone for cations, MES for anions) and homogenized for 1 min to inactivate enzymes. Then, deionized water (500 μl) was added, 300 μl of the solution were transferred to another tube, and 200 μl of chloroform were added, and the mixture thoroughly mixed. The solution was centrifuged at 12,000 × *g* for 15 min at 4 °C, and the 300-μl upper aqueous layer was centrifugally filtered through a Millipore 5-kDa cutoff filter to remove proteins. The filtrate was lyophilized and dissolved in 50 μl of Milli-Q water containing reference compounds (200 μM each of 3-aminopyrrolidine and trimesate) prior to CE-TOFMS analysis.

For serum studies, 200-μl samples were plunged into 1.8 ml of methanol containing 55 μM each of methionine sulfone and MES and mixed well. Then 800 μl of deionized water and 2 ml of chloroform were added, and the solution was centrifuged at 2,500 × *g* for 5 min at 4 °C. The 800-μl upper aqueous layer was centrifugally filtered through a Millipore 5-kDa cutoff filter to remove proteins. Subsequent steps were as for liver samples.

Metabolite Standards—All chemical standards were obtained from common commercial sources and dissolved in Milli-Q (Millipore, Bedford, MA) water, 0.1 N HCl or 0.1 N NaOH to obtain 10 mM or 100 mM stock solutions. Working standard mixtures were prepared by diluting stock solutions with Milli-Q water just prior to injection into the CE-TOFMS. The chemicals used were of analytical or reagent grade.

Instrumentation—All CE-TOFMS experiments were performed using an Agilent CE capillary electrophoresis system (Agilent Technologies, Waldbronn, Germany), an Agilent G3250AA LC/MSD TOF system (Agilent Technologies, Palo Alto, CA), an Agilent1100 series binary HPLC pump, and the G1603A Agilent CE-MS adapter and G1607A Agilent CE-ESI-MS sprayer kit. For system control and data acquisition we used the G2201AA Agilent ChemStation software for CE and the Analyst QS for Agilent TOFMS software. CE-MS/MS analyses for compound identification were performed on a Q-Star XL Hybrid LC-MS/MS System (Applied Biosystems, Foster City, CA) connected to an Agilent CE instrument.

CE-TOFMS Conditions for Cationic Metabolite Analysis—Separations were carried out in a fused silica capillary (50 μm inner diameter × 100 cm total length) filled with 1 M formic acid as the electrolyte (21). Approximately 3 nl of sample solution were injected at 50 mbar for 3 s, and 30 kV of voltage was applied. The capillary temperature was maintained at 20 °C, and the sample tray was cooled below 5 °C. Methanol-water (50% v/v) containing 0.5 μM reserpine was delivered as the sheath liquid at 10 μl/min. ESI-TOFMS was operated in the positive ion mode, and the capillary voltage was set at 4,000 V. A flow rate of heated dry nitrogen gas (heater temperature 300 °C) was maintained at 10 psig. In TOFMS, the fragmentor, skimmer, and Oct RFV voltage were set at 75 V, 50 V, and 125 V, respectively. Automatic recalibration of each acquired spectrum was performed using reference masses of reference standards. The methanol adduct ion ($[2MeOH + H_2O + H]^+$, m/z 83.0703) and reserpine ($[M + H]^+$, m/z 609.2806) provided the lock mass for exact mass measurements. Exact mass data were acquired at a rate of 10 spectra/s over a 50–1,000 m/z range.

CE-TOFMS Conditions for Anionic Metabolite Analysis—A cationic polymer-coated SMILE (+) capillary (22) (Nacalai Tesque, Kyoto, Japan) was used as the separation capillary (23). A 50 mM ammonium acetate solution (pH 8.5) was used as electrolyte solution for CE separation. Sample solution (30 nl) was injected at 50 mbar for 30 s and −30 kV of voltage was applied. Ammonium acetate (5 mM) in 50% methanol-water (v/v) containing 20 μM PIPES and 1 μM reserpine was delivered as the sheath liquid at 10 μl/min. ESI-TOFMS was conducted in the negative ion mode; the capillary voltage was set at 3,500 V. For TOFMS, the fragmentor, skimmer, and Oct RFV voltage were set at 100 V, 50 V, and 200 V, respectively. Automatic recalibration of each acquired spectrum was performed using reference masses of standards, *i.e.* divalent PIPES ($[M - 2H]^{2-}$, m/z 150.0230), monovalent PIPES ($[M - H]^-$, m/z 301.0534), and reserpine ($[M - H]^-$, m/z 607.2661). Other conditions were identical to those used in cationic metabolite analysis.

CE-Q-TOFMS Conditions for the Acquisition of MS/MS Spectra—Most of the conditions were identical to those in cationic metabolite analysis using CE-TOFMS. Methanol-water (50% v/v) containing 1 μM reserpine was delivered as the sheath liquid at 5 μl/min. ESI-Q-TOFMS was conducted in the positive product ion scan mode; the ion spray voltage was set at 5,500V. Dry air (GS1) was maintained at 10 psi. The declustering potential 1 and 2, and the collision energy voltage were set at 60 V, 15 V, and 20 V, respectively. Recalibration was manually performed with reserpine ($[M + H]^+$, m/z 609.2806) and its fragment ion ($[M + H]^+$, m/z 195.0652).

Data Processing for the Generation of the Metabolome Differential Display—Raw datasets were preprocessed by binning the data along the m/z axis to 0.02 m/z resolution, subtracting the baseline from each electropherogram by robust nonlinear fitting of the data to a 7th order polynomial and removing the noise from each electropherogram by leveling to 0 all signal intensity values that fell within 5× S.D. of the signal intensities from 1 to 4 min. The resulting data sets were then further binned to 1 m/z unit resolution along the m/z axis. A set of peaks was selected from each dataset using a modified Douglas-Peucker algorithm (24); alignment of datasets along the migration time axis was as described in the text. Annotation tables for both cation and anion modes were generated based on the results of the CE-TOFMS analysis of standard compounds. The annotation labels were aligned to the actual datasets in a similar fashion. Arithmetic operations were applied to whole datasets on a data point-by-data point basis to highlight differences of interest. Averaging the datasets within each group allowed visualization of absolute (difference between the corresponding intensities from the averaged datasets) and relative (absolute difference divided by the larger of the two corresponding intensities) differences. To generate the metabolome differential displays shown in Fig. 1 and supplemental Fig. S1, the product of two results was used so that differences significant in both absolute and relative terms were preferentially visualized. Overlaid electropherograms in the vicinity of the most significant differences from the results of interest were plotted in descending order of significance for visual confirmation. A Mathematica (Wolfram Research Inc.) package for differential analysis of metabolite profiles, a detailed description of which is beyond the scope of this manuscript, will be released separately.

RESULTS AND DISCUSSION

Development of Metabolome Differential Display—By coupling a CE system with an Agilent TOFMS instrument, we developed a new analytical system for metabolome differential display. Because TOFMS instruments are usually calibrated to analyze macromolecules like peptides and proteins, we first optimized the settings of the ion guide optics, *i.e.* the fragmentor, skimmer, and Oct RFV voltage for the analysis of low molecular mass substances (50–1,000 Da). This optimization enabled the sensitive detection of small molecules. To measure the system's reliability, we then analyzed 338 cations by CE-TOFMS and measured the errors in mass accuracy. These errors were nonlinearly related to the m/z values and were less than 10 ppm in the range from 200 to 400 m/z and less than 30 ppm outside this range (see Fig. 2*A*). Because errors in

Downloaded from www.jbc.org at Biomedical Library, UCSD, on February 25, 2011

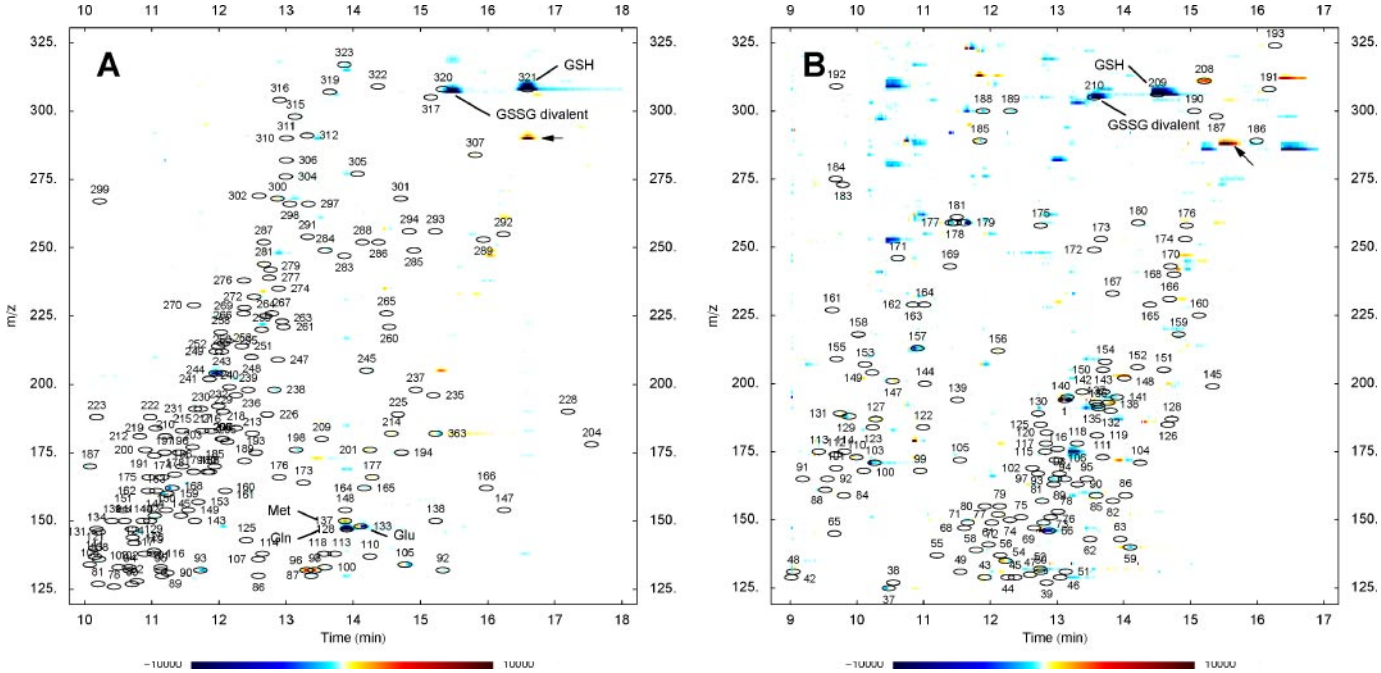

FIGURE 1. **View of metabolome differential displays.** Cations (*A*) and anions (*B*) obtained from CE-TOFMS analyses of livers of control mice ($n = 5$) and mice 2 h after intraperitoneal injection with AAP ($n = 5$). The plots were generated as described under "Materials and Methods," and the position of standard compounds is overlaid with the differential profiles and numbers correspond to compounds listed in supplemental Table S2. The *arrow* points to the metabolite (later identified as ophthalmate) whose level significantly increased ($p < 0.05$) in AAP-treated mice. Anion peaks 208, 209, and 210 on *plot B* were identified by CE-TOFMS as mercapturate, GSH, and GSSG divalent ion. The gradation of the color bar indicates the increase (*red*) or the decrease (*blue*) of the metabolite level after AAP administration.

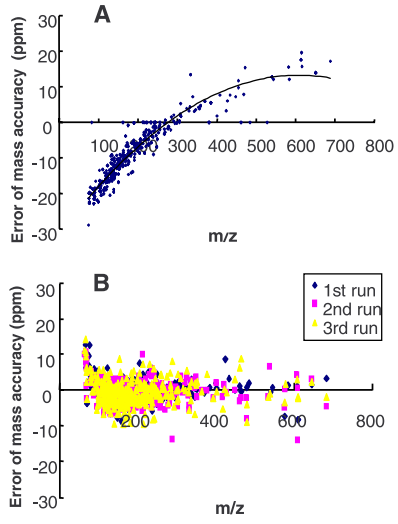

FIGURE 2. **Mass accuracy for triplicate measurements of a mixture of 338 cations (20 μM each) obtained by CE-TOFMS.** *A*, standard mass calibration before analysis or *B*, real-time recalibration for every mass spectrum using the sheath liquid calibrant method (*blue*, *magenta*, and *yellow* colors indicate the results obtained by 1st, 2nd, and 3rd run, respectively).

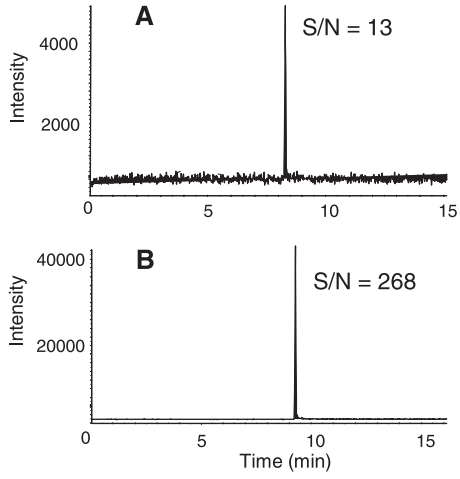

FIGURE 3. **CE-TOFMS sensitivity for arginine (10 μM).** *A*, the reference sprayer recalibration (signal-to-noise ratio, S/N = 13) and *B*, the sheath liquid recalibration method (S/N = 268) are shown.

TOFMS measurements seemed to be attributed to real time fluctuations in environmental conditions such as temperature and vacuum, we opted to constantly deliver a calibrant solution using a reference sprayer (second sprayer) provided with the Agilent TOFMS system, and recalibrated the mass axis for each spectrum using the measurement of known reference masses (*i.e.* "lock masses") (25). Although this lock-mass spray improved the mass accuracy, detection sensitivity decreased considerably (Fig. 3*A*). We believe that this decrease in sensitivity may be because of interference by the reference sprayer and/or to dilution of analyte solution (several μl/min) in the calibrant solution (100 μl/min).

To overcome this problem, we added reserpine (mass recalibration standard) directly to the sheath solution, used to assist electrospray ionization (flow rate 10 μl/min). In addition to the spiked reserpine standard ($[M + H]^+$, m/z 609.2806) the methanol adduct ion ($[2MeOH + H_2O + H]^+$, m/z 83.0730) found in the sheath solution was also used as another calibrant. This procedure provided mass accuracies within 10 ppm for almost all compounds (Fig. 2*B*) and a more than 20-fold increase in sensitivity (Fig. 3*B*). Similarly, we recalibrated the mass accuracy for anionic compounds using a sheath liquid containing three calibrants, *i.e.* divalent PIPES ($[M - 2H]^{2-}$, m/z 150.0230), monovalent PIPES ($[M - H]^-$, m/z 301.0534), and reserpine ($[M - H]^-$, m/z 607.2661), yielding satisfactory results (data not shown).

Next, we validated the CE-TOFMS methods using amino acids or phosphorylated compounds as representatives of cationic and anionic metabolites, respectively. Good reproducibility, linearity, and sensitivity were obtained (see supplemental Table S1). Specially, the detection lim-

Downloaded from www.jbc.org at Biomedical Library, UCSD, on February 25, 2011

its for most amino acids and anionic species in CE-TOFMS were improved on average severalfold and as much as 65-fold over previously reported values for the CE-quadrupole mass spectrometer (QMS) (21, 23). We attribute this significant increase in sensitivity to the fact that TOFMS allows more ions to reach the detector during the instrument duty cycle and that the exact mass resolution of the TOF instrument results in a considerable reduction in the baseline noise.

To facilitate the analysis and comparison of large and complex data sets produced by CE-MS analysis, visualization tools are desirable. Few available tools exist to do this, especially for CE-MS data where migration time variations between samples are significant. An important issue in the development of a differential displays tool is thus the normalization of the compound migration times. The function derived by Reijenga *et al.* (26) for electropherogram normalization in CE fit the shifts in migration times between corresponding peaks from different data sets. To align the peaks from two CE-MS data sets, the sum of dynamic programming (DP) scores, serving as a measure of the quality of the alignment, was calculated for all corresponding electropherograms. Partial scores (or gap penalty values) were assigned to the distance between two peaks of a subproblem and the Reijenga function parameters were optimized to achieve the lowest overall DP score (Fig. 4). The time scale of the sample data set was then rescaled to that of the reference and signal intensities were adjusted accordingly to compensate for the compression or expansion of the peaks, thereby conserving their original peak areas.

Differential Display of Liver Metabolites in Acetaminophen-treated Mice—To evaluate the power of our metabolite profiling and differential display methods to pin-point changes in the metabolome in an unbiased manner and identify biomarkers, we determined the changes in murine hepatic metabolite levels after AAP administration. To facilitate the assignment of specific metabolites to peaks, we first analyzed 569 metabolic standards listed in the KEGG LIGAND data base (27) by CE-TOFMS before analyzing tissue-derived samples. Global mass scanning over a 50–1,000 m/z range was applied in both cation and anion CE modes. Almost all compounds were well resolved and were annotated with numbers referring to the compound list (supplemental Fig. S1, *A* and *B* and supplemental Table S2). To study the effects of AAP on liver metabolism, we determined liver metabolite levels two hours (control, supplemental Fig. S1, *C* and *D*) after injection with either saline or AAP (point where liver damage is maximum, supplemental Fig. S1, *E* and *F*). Our metabolome differential data analysis tool automatically normalized the migration times of all peaks in the samples and matched these with the standard annotation table. This allowed to readily identify the corresponding peaks. A total of 132 metabolites were identified among 1,859 detected peaks (supplemental Table S3).

Among the several changes, differential display of liver metabolites between the controls and AAP treated (2 h) showed extensive depletion of GSH and its oxidized form (GSSG), detected as a divalent ion (Fig. 1). In paired Student's t tests, the level of 13 identifiable metabolites were significantly different ($p < 0.01$), and most were part of metabolic processes proximal to glutathione biosynthesis such as the transsulfuration pathway, taurine shunt, and remethylation cycles (supplemental Table S3). As seen when plotting results on the glutathione biosynthesis pathways (Fig. 5*A*), the level of most of these metabolites decreased at 2-h post-AAP treatment. These metabolite changes are likely linked to the GSH depletion by conjugation (oxidation) with NAPQI, and the associated depletion of intermediates for glutathione biosynthesis. On the other hand, the level of methionine, an essential amino acid located upstream in the cysteine synthesis pathway, more than doubled in AAP-treated mice. This alteration could be the result of the AAP-elicited

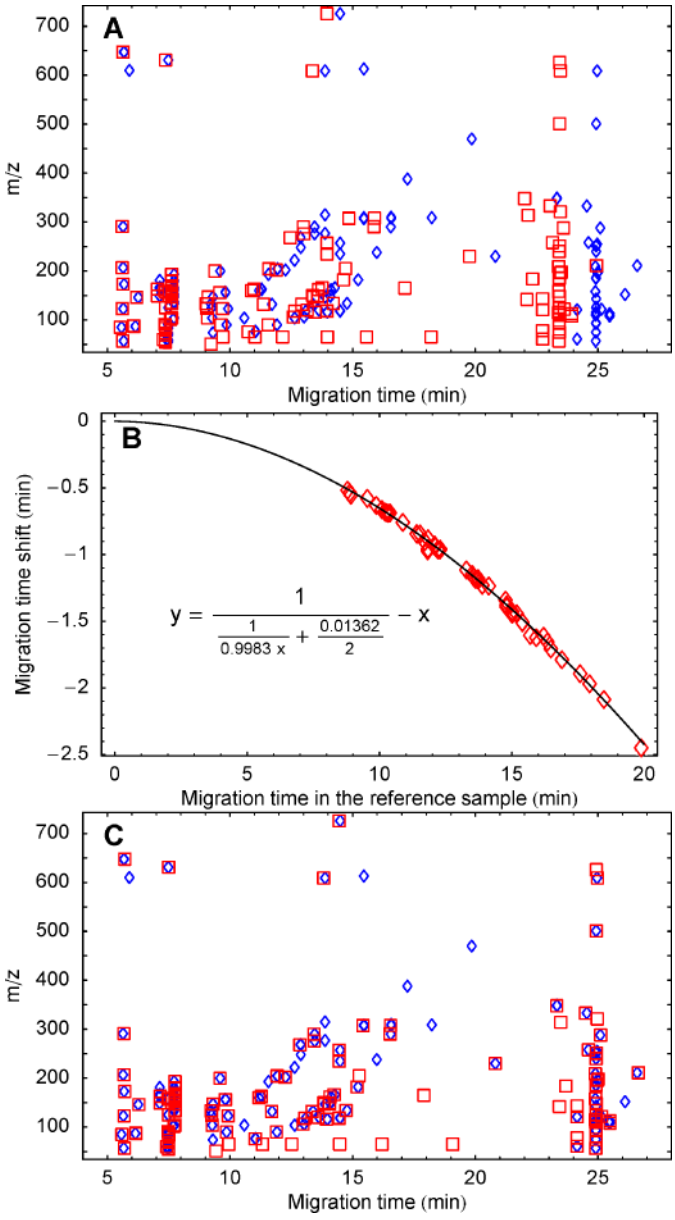

FIGURE 4. **Alignment of two datasets.** *A*, *blue diamonds* and *red squares* show the position of peaks obtained from one of the control sample datasets and one of the AAP-treated sample datasets, respectively. *B*, migration time shifts between corresponding peaks from the two datasets were fitted to the Reijenga's function as described in the main text. *C*, function was then used to rescale the timescale of the AAP treatment sample dataset.

decrease in GSH, which is a necessary cofactor for methionine adenosyltransferase (MAT) (28). Alternately, a possible inhibition of cystathionine β-synthase, the rate-limiting enzyme in the transsulfuration pathway might explain this finding. This can be suggested from the elevation of both methionine and serine levels without a concomitant increase in cystathionine levels at 2–6 h after AAP exposure (supplemental Fig. S3), although the detailed mechanism requires further examination.

Another major change in metabolite profiles of AAP-treated mice was the significant increase in abundance of an unidentified cationic metabolite of m/z 290.135 eluting at 16.5 min (Fig. 1) whose characterization is described in detail below.

Ophthalmate as Major Byproduct after AAP Treatment and Activation of Its Biosynthesis—Using tandem mass spectrometry with a CE-Q-TOFMS system, the precise MS/MS spectra of GSH (Fig. 6*A*) and the

Downloaded from www.jbc.org at Biomedical Library, UCSD, on February 25, 2011

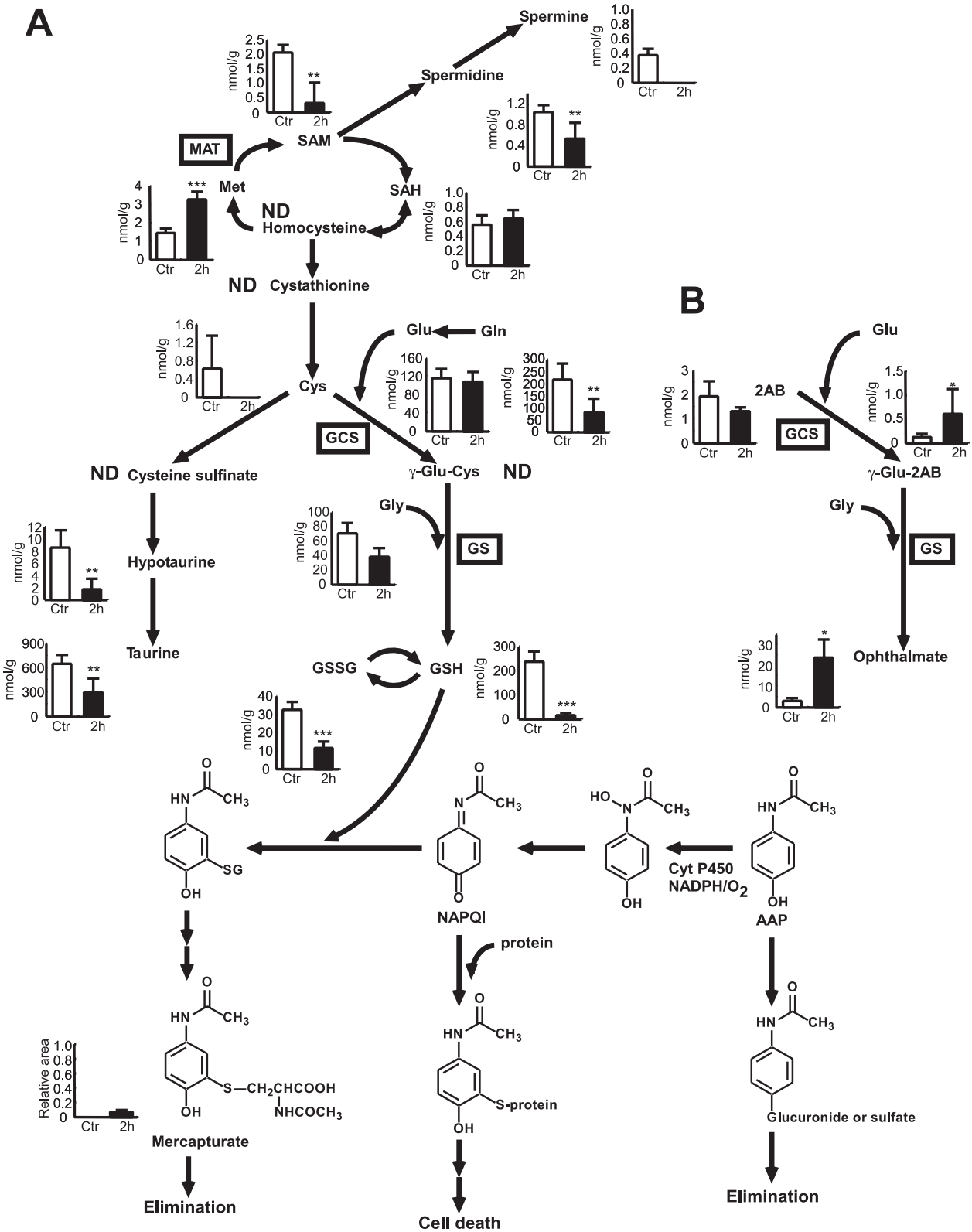

FIGURE 5. **Observed metabolite changes mapped onto the pathways involved in acetaminophen metabolism and its elimination.** *A*, changes in hepatic metabolite levels in the controls and mice injected 2 h earlier with AAP. The data were obtained by simultaneous analysis of charged metabolites using CE-TOFMS and correspond to the data shown in Fig. 1. *B*, changes in hepatic metabolite levels in the controls and mice injected 2 h earlier with AAP. The metabolites participate in the part of the pathway leading to ophthalmate biosynthesis. *Asterisks* indicate statistically significant differences. ***, $p < 0.001$; **, $p < 0.01$; *, $p < 0.05$.

unknown cation (*m*/*z* 290.135, 16.5 min) (Fig. 6*B*) obtained by CE-Q-TOFMS analysis of liver samples were carefully compared. The fragmentation patterns of GSH and the unknown cation were similar, and the mass difference between the four predominant peaks was just around 17.96 Da (indicated by *red dashed arrows* in Fig. 6). This suggested that the SH (32.980 Da) group in GSH might be replaced by a

Downloaded from www.jbc.org at Biomedical Library, UCSD, on February 25, 2011

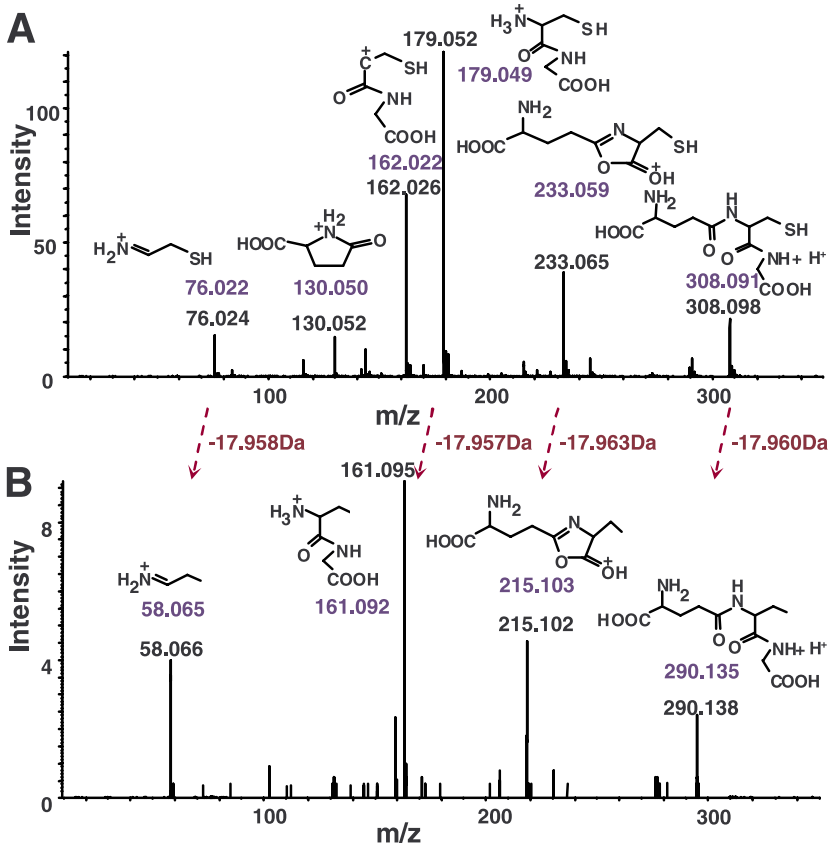

FIGURE 6. **MS/MS spectra of (*A*) GSH and (*B*) an unknown cation (*m/z* 290. 0135, 16.5 min) by CE-Q-TOFMS.** The chemical structures of the fragment ions and their *m/z* values (*blue*) (see supplemental Fig. S2), and the experimentally obtained *m/z* values for fragment ions (*black*) are displayed. The fragmentation patterns between GSH and the unknown cation are similar, and the mass difference between the four dominant peaks is close to 17.96 Da (*red dashed arrows*).

CH_3 (15.023 Da) group (32.980–15.023 Da = 17.957 Da) in the unknown compound. To confirm the position of the substitution within the GSH tripeptide (γ-Glu-Cys-Gly), we compared the MS/MS fragmentation pattern of both GSH and the unknown cation, the latter based on the structure of ophthalmate (see supplemental Fig. S2). We compared the *m/z* values of the predominant ions in the resulting compound (blue) with those from the experimentally determined MS/MS fragmentation ions (black) (Fig. 6, *A* and *B*) to assess their consistency. The results are consistent with the replacement of the SH group of the cysteine residue of GSH, with a CH_3 group to form 2-aminobutyrate (2AB) found in ophthalmate (γ-Glu-2AB-Gly). To confirm this, we obtained ophthalmate from commercial sources (Bachem, Bubendorf, Switzerland) and analyzed mouse liver samples spiked with the ophthalmate standard using CE-TOFMS and CE-Q-TOFMS. There was a perfect correspondence with respect to both migration time and MS/MS spectrum between ophthalmate and the unknown compound. This result thus leads us to conclude that the unidentified compound is indeed ophthalmate.

As ophthalmate is an analog of GSH, this finding raises the question of how the thiol group of cysteine in GSH is replaced by a methyl group in ophthalmate. As for GSH, ophthalmate can be synthesized *in vivo* from 2AB through consecutive reactions with γ-glutamylcysteine synthetase (GCS) and glutathione synthetase (GS) (Fig. 5*B*) (29). Further support for this biosynthetic route comes from previous reports that GCS catalyzes the ligation of glutamine and 2AB (30) and that GS can synthesize ophthalmate from γ-Glu-2AB (31). In agreement with this, the level of γ-Glu-2AB (*m/z* 233.113, 15.5 min), a substrate of GS, increased in the liver of AAP-treated mice (Fig. 5*B*). This finding suggests that GCS, the enzyme that is feedback-inhibited by GSH, and is a rate-limiting step in GSH synthesis (32, 33), was activated during GSH depletion and/or that GS may display lower affinity for γ-Glu-2AB compared with γ-Glu-Cys.

We further investigated ophthalmate metabolism by lowering the hepatic content of GSH by pretreating mice with BSO or DEM (Fig. 7*A*). BSO is known to result in significant GCS inhibition (34) and thus cause a reduction of downstream products. On the other hand, DEM leads to the oxidation of the thiol group in GSH (35) and the induction of lipid peroxidation and necrotic cell death (36). Liver and serum samples from control and BSO and DEM treated mice were analyzed in more detail by CE-TOFMS to identify specific changes in the levels of GSH/GSSG and ophthalmate and its precursors. As expected, the levels of GSH as well as γ-Glu-2AB and ophthalmate were very low both in the liver and serum of GCS-inhibited mice (Fig. 7, *A* and *B*). On the other hand, a marked increase in γ-Glu-2AB and ophthalmate levels was seen in DEM-treated mice. We can thus conclude that ophthalmate was synthesized using the same pathway as GSH. The results also suggest that GSH depletion by oxidative compounds such as AAP and DEM resulted in GCS activation, which in turn induced ophthalmate synthesis. However, unlike GSH, ophthalmate was not further metabolized and thus accumulated (Fig. 8).

Ophthalmate as an Oxystress Biomarker Indicating GSH Depletion—The above results in BSO- and DEM-treated mice indicate that a significant portion of these liver metabolites were effluxed to the circulation by the action of ATP-binding cassette (ABC) transporters such as multidrug resistance proteins (37) (Fig. 8). This close correspondence between hepatic and serum levels suggests the possibility that some of the detected compounds could act as biomarkers of GSH level alteration. In addition, the fact that both AAP and DEM result in GSH depletion and an increase in ophthalmate levels suggests that this response is not specific to AAP treatment but possibility reflects a more general cellular response to oxidative stress.

Downloaded from www.jbc.org at Biomedical Library, UCSD, on February 25, 2011

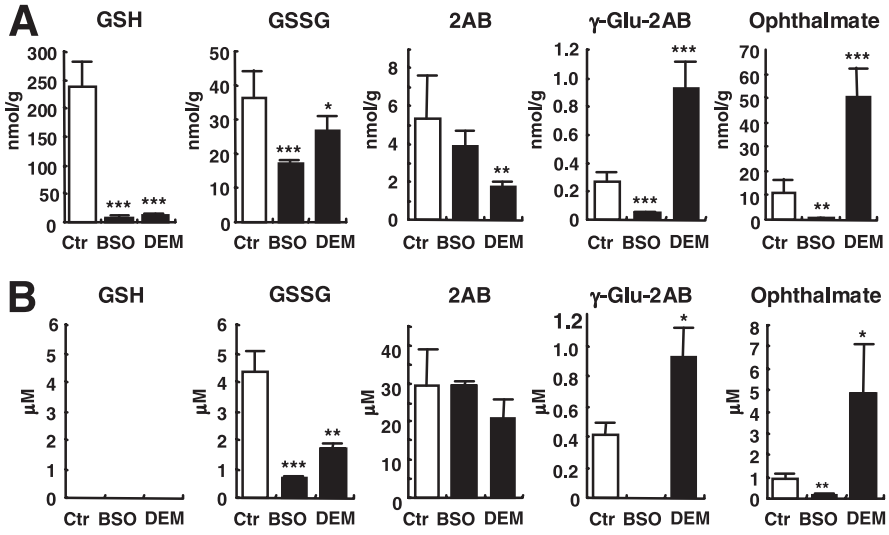

FIGURE 7. **Metabolite concentrations in (*A*) mouse liver ($n = 5$) and (*B*) serum ($n = 3$) 2 h after BSO or DEM treatment obtained by CE-TOFMS.** *Asterisks* indicate significant differences. ***, $p < 0.001$; **, $p < 0.01$; *, $p < 0.05$. No γ-Glu-Cys peak was detected.

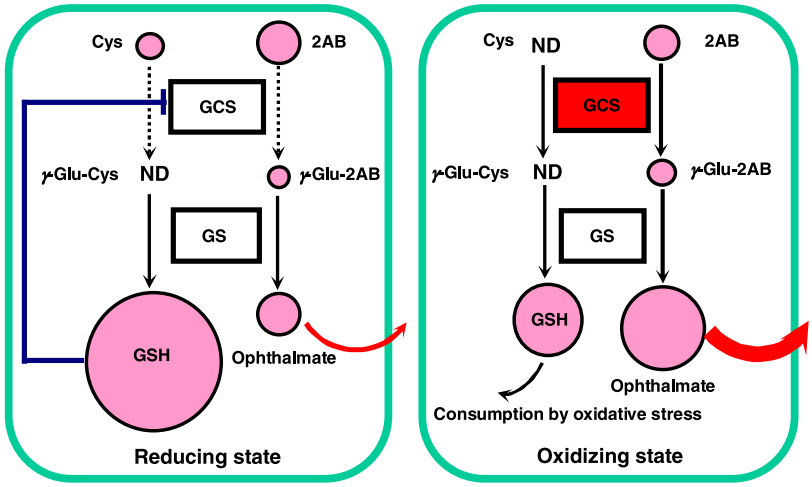

FIGURE 8. **Mechanism of ophthalmate biosynthesis in hepatocytes.** GCS is feedback-inhibited by GSH under reducing condition and little ophthalmate is thus synthesized. During oxidative stress, GSH is consumed, leading to GCS activation. This could result in biosynthesis of ophthalmate which is then effluxed across hepatocellular membrane through MRP transporters. The size of metabolite circles is proportional to their measured abundance in liver. *ND*, not detected.

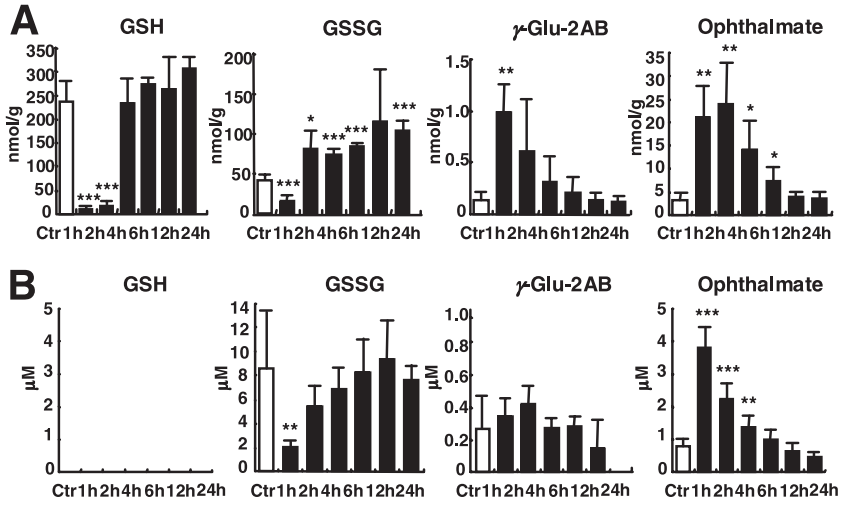

FIGURE 9. **Changes in metabolite levels in (*A*) mouse liver and (*B*) serum 1, 2, 4, 6, 12, and 24 h after AAP treatment ($n = 4$).** *Asterisks* indicate significant differences (***, $p < 0.001$; **, $p < 0.01$; *, $p < 0.05$). The hepatic GSH level at 1 h after AAP treatment was ~28-times lower than in the controls ($p < 1.6 \times 10^{-5}$). On the other hand, the ophthalmate level in mouse serum at 1 h after AAP treatment increased ~5-fold compared with the controls ($p = 0.0001$).

GSH, a ubiquitous and important antioxidant that protects mitochondria against endogenous oxygen radicals, is one of the most abundant intracellular antioxidants (38). GSH maintains enzymes and other cellular components in a reduced state (39) and its depletion leads to cell death. Therefore, biomarkers that can reveal disturbances in intracellular GSH levels can provide important information on the cellular reduction-oxidation (redox) state. We measured the levels of GSH, GSSG, γ-Glu-2AB, and ophthalmate, together with several metabolic intermediates of glutathione biosynthesis, in both liver and serum of mice at 1, 2, 4, 6, 12, and 24 h after AAP treatment. Most of the monitored metabolites that were detected in liver were also present in serum, but there was no significant difference in their concentration between control and AAP-treated mice (supplemental Fig. S3). On the other hand, significant increases in liver and serum ophthalmate levels were observed with

Downloaded from www.jbc.org at Biomedical Library, UCSD, on February 25, 2011

a concurrent hepatic GSH depletion in AAP treated mice (Fig. 9). Despite the high GSH levels in liver, GSH was not detected in serum suggesting that GSH is either not effluxed from liver, or that it is rapidly metabolized or oxidized in serum (40).

Serum ophthalmate increased ~5-fold ($p = 0.0001$) 1 h after AAP treatment, a point at which the liver GSH level dropped dramatically (Fig. 9). The change in hepatic ophthalmate was inversely proportional to the hepatic GSH level. These results thus identify serum ophthalmate level as a potential hepatic GSH biomarker that can reveal liver GSH abnormalities triggered by oxidative stress (Fig. 8).

Whereas hepatic γ-Glu-2AB increased 1 h after AAP treatment, serum γ-Glu-2AB did not increase significantly (Fig. 9), indicating that hepatic γ-Glu-2AB may not readily be exported to the circulation by ABC transporters or that, similarly to GSH, it is rapidly metabolized.

Overall, the time frame of changes in metabolites that we observed agrees very well with a previous report (9) showing a rapid (1–2 h) induction of multiple hepatic genes and their products following AAP administration in the mouse.

The physiological role of ophthalmate is not clearly established. In this work, it appears to be produced as a byproduct of the GS reaction when GSH, and consequently, cysteine levels are depleted. However, it has been previously suggested that ophthalmate may act as an anti-coenzyme (41) that can inhibit enzymes that use GSH as a co-factor. GSH is normally exported in large proportion by the liver into bile and circulation to be used in peripheral tissues (42). Interestingly, ophthalmate was shown to competitively inhibit and trans-stimulate GSH uptake in liver canalicular membranes (43). This may help minimize GSH efflux from liver cells during oxidative stress.

GSH is conjugated to many types of exogenous metabolites such as AAP to increase their solubility and facilitate their excretion. GSH also enhances multidrug resistance protein 1 (MRP1)-mediated transport of the glucoronide conjugate of the tobacco carcinogen 4-(methylnitrosamino)-1-(3-pyridyl)-1-butanol (NNAL) and ophthalmate can substitute for this activity (44, 45). Ophthalmate can thus act as a GSH analog for functions that do not require the presence of the thiol group such as activation of transport of exogenous metabolite glucoronides by MRP1. It is thus tempting to speculate that ophthalmate might similarly stimulate the transport of AAP-glucoronide by MRP1 and thus facilitate its elimination. This would provide functional meaning for its synthesis during oxidative stress rather than simply being a consequence or byproduct of cysteine/GSH depletion and the associated activation of GCS.

Because of differences in the analytical methods, our results seem complementary to previous work by Coen *et al.* (46, 47) who profiled changes in liver metabolites following AAP treatment using NMR. Whereas these authors examined mostly neutral and lipid metabolites, our work using CE-MS and focusing on polar metabolites demonstrates the consequences of GSH depletion and the attempts of the liver to increase its biosynthesis. On the other hand, Coen *et al.* (46, 47) reported an activation of glycolysis while lipid metabolism was decreased and this may reflect the energy and precursor requirements for GSH and related metabolites biosynthesis as well as mitochondrial damage, respectively. Both studies concur regarding increases in the level of several amino acids, which can be measured by both NMR and CE-TOFMS levels.

We presented a sensitive and high resolution metabolome differential display approach, based on a CE-TOFMS system and data analysis software, that facilitates the global quantification and identification of charged metabolites as well as the visualization of specific changes in complex biological matrices. This approach can be applied to the discovery of biomarkers as we demonstrated by the identification of serum ophthalmate as a biomarker for hepatic GSH depletion following oxidative stress. Ophthalmate measurement can potentially provide valuable information about the hepatic cellular redox state, thereby facilitating the earlier prediction of oxidative damage. This biomarker may thus help to evaluate therapeutic risks, efficacy, and drug actions during the drug development process and potentially facilitate the early detection of several diseases (such as Alzheimers, Parkinsons, and liver disease, AIDS, cancer, cardiac infarction, and diabetes) (48), where oxidative stress is known to play an important role.

Acknowledgments—We thank Kenjiro Kami, Natsumi Saito, Masahiro Sugimoto, Noriyuki Sugiyama, and Mineo Morohashi for technical advice and support.

REFERENCES

1. Vermeulen, N. P., Bessems, J. G., and Van de Straat, R. (1992) *Drug Metab. Rev.* **24,** 367–407
2. Dahlin, D. C., Miwa, G. T., Lu, A. Y., and Nelson, S. D. (1984) *Proc. Natl. Acad. Sci. U. S. A.* **81,** 1327–1331
3. Vendemiale, G., Grattagliano, I., Altomare, E., Turturro, N., and Guerrieri, F. (1996) *Biochem. Pharmacol.* **52,** 1147–1154
4. Mitchell, J. R., Jollow, D. J., Potter, W. Z., Davis, D. C., Gillette, J. R., and Brodie, B. B. (1973) *J. Pharmacol. Exp. Ther.* **187,** 185–194
5. Gibson, J. D., Pumford, N. R., Samokyszyn, V. M., and Hinson, J. A. (1996) *Chem. Res. Toxicol.* **9,** 580–585
6. Wallace, J. L. (2004) *Br. J. Pharmacol.* **143,** 1–2
7. Hinson, J. A., Reid, A. B., McCullough, S. S., and James, L. P. (2004) *Drug Metab. Rev.* **36,** 805–822
8. Reilly, T. P., Bourdi, M., Brady, J. N., Pise-Masison, C. A., Radonovich, M. F., George, J. W., and Pohl, L. R. (2001) *Biochem. Biophys. Res. Commun.* **282,** 321–328
9. Ruepp, S. U., Tonge, R. P., Shaw, J., Wallis, N., and Pognan, F. (2002) *Toxicol. Sci.* **65,** 135–150
10. Raamsdonk, L. M., Teusink, B., Broadhurst, D., Zhang, N., Hayes, A., Walsh, M. C., Berden, J. A., Brindle, K. M., Kell, D. B., Rowland, J. J., Westerhoff, H. V., van Dam, K., and Oliver, S. G. (2001) *Nat. Biotechnol.* **19,** 45–50
11. Spinnler, H. E., Ginies, C., Khan, J. A., and Vulfson, E. N. (1996) *Proc. Natl. Acad. Sci. U. S. A.* **93,** 3373–3376
12. Ideker, T., Thorsson, V., Ranish, J. A., Christmas, R., Buhler, J., Eng, J. K., Bumgarner, R., Goodlett, D. R., Aebersold, R., and Hood, L. (2001) *Science* **292,** 929–934
13. Fraenkel, D. G. (1992) *Annu. Rev. Genet.* **26,** 159–177
14. Fernie, A. R., Trethewey, R. N., Krotzky, A. J., and Willmitzer, L. (2004) *Nat. Rev. Mol. Cell. Biol.* **5,** 763–769
15. Fiehn, O., Kopka, J., Dormann, P., Altmann, T., Trethewey, R. N., and Willmitzer, L. (2000) *Nat. Biotechnol.* **18,** 1157–1161
16. Plumb, R., Granger, J., Stumpf, C., Wilson, I. D., Evans, J. A., and Lenz, E. M. (2003) *Analyst* **128,** 819–823
17. Reo, N. V. (2002) *Drug Chem. Toxicol.* **25,** 375–382
18. Aharoni, A., Ric de Vos, C. H., Verhoeven, H. A., Maliepaard, C. A., Kruppa, G., Bino, R., and Goodenowe, D. B. (2002) *Omics* **6,** 217–234
19. Soga, T., Ohashi, Y., Ueno, Y., Naraoka, H., Tomita, M., and Nishioka, T. (2003) *J. Proteome. Res.* **2,** 488–494
20. Shiomi, M., Wakabayashi, Y., Sano, T., Shinoda, Y., Nimura, Y., Ishimura, Y., and Suematsu, M. (1998) *Hepatology* **27,** 108–115
21. Soga, T., and Heiger, D. N. (2000) *Anal. Chem.* **72,** 1236–1241
22. Katayama, H., Ishihama, Y., and Asakawa, N. (1998) *Anal. Chem.* **70,** 5272–5277
23. Soga, T., Ueno, Y., Naraoka, H., Ohashi, Y., Tomita, M., and Nishioka, T. (2002) *Anal. Chem.* **74,** 2233–2239
24. Douglas, D. H., and Peucker, T. K. (1973) *Can. Cartographer* **10,** 112–122
25. Palmer, M. E., Clench, M. R., Tetler, L. W., and Little, D. R. (1999) *Raid Commun. Mass Spectrom.* **13,** 256–263
26. Reijenga, J. C., Martens, J. H. P. A., Giuliani, A., and Chiari, M. (2002) *J. Chromatogr. B* **770,** 45–51
27. Goto, S., Okuno, Y., Hattori, M., Nishioka, T., and Kanehisa, M. (2002) *Nucleic Acids Res.* **30,** 402–404
28. Corrales, F. J., Ruiz, F., and Mato, J. M. (1999) *J. Hepatol.* **31,** 887–894
29. Orlowski, M., and Wilk, S. (1978) *Biochem. J.* **170,** 415–419
30. Huang, C. S., Moore, W. R., and Meister, A. (1988) *Proc. Natl. Acad. Sci. U. S. A.* **85,** 2464–2468
31. Oppenheimer, L., Wellner, V. P., Griffith, O. W., and Meister, A. (1979) *J. Biol. Chem.* **254,** 5184–5190
32. Richman, P. G., and Meister, A. (1975) *J. Biol. Chem.* **250,** 1422–1426

Downloaded from www.jbc.org at Biomedical Library, UCSD, on February 25, 2011

33. Cuozzo, J. W., and Kaiser, C. A. (1999) *Nat. Cell Biol.* **1,** 130–135
34. Griffith, O. W., and Meister, A. (1979) *J. Biol. Chem.* **254,** 7558–7560
35. Zalups, R. K., and Lash, L. H. (1997) *Drug Metab. Dispos.* **25,** 516–523
36. Tirmenstein, M. A., Nicholls-Grzemski, F. A., Zhang, J. G., and Fariss, M. W. (2000) *Chem. Biol. Interact.* **127,** 201–217
37. Keppler, D., Leier, I., and Jedlitschky, G. (1997) *Biol. Chem.* **378,** 787–791
38. Yang, C. S., Chen, W. Y., Tsai, P. J., Cheng, F. C., and Kuo, J. S. (1997) *Biochem. Pharmacol.* **53,** 357–361
39. Meister, A. (1995) *Methods Enzymol.* **251,** 3–7
40. Joshi, U. M., Rao, K. S., and Mehendale, H. M. (1987) *Int. J. Biochem.* **19,** 1029–1035
41. Waley, S. G. (1953) *Biochim. Biophys. Acta* **10,** 27–34
42. Meister, A., and Anderson, M. E. (1983) *Annu. Rev. Biochem.* **52,** 711–760
43. Ballatori, N., and Dutczak, W. J. (1994) *J. Biol. Chem.* **269,** 19731–19737
44. Leslie, E. M., Ito, K., Upadhyaya, P., Hecht, S. S., Deeley, R. G., and Cole, S. P. (2001) *J. Biol. Chem.* **276,** 27846–27854
45. Leslie, E. M., Bowers, R. J., Deeley, R. G., and Cole, S. P. (2003) *J. Pharmacol. Exp. Ther.* **304,** 643–653
46. Coen, M., Lenz, E. M., Nicholson, J. K., Wilson, I. D., Pognan, F., and Lindon, J. C. (2003) *Chem. Res. Toxicol.* **16,** 295–303
47. Coen, M., Ruepp, S. U., Lindon, J. C., Nicholson, J. K., Pognan, F., Lenz, E. M., and Wilson, I. D. (2004) *J. Pharm. Biomed. Anal.* **35,** 93–105
48. Wu, G., Fang, Y. Z., Yang, S., Lupton, J. R., and Turner, N. D. (2004) *J. Nutr.* **134,** 489–492

Downloaded from www.jbc.org at Biomedical Library, UCSD, on February 25, 2011